Impact of trypsin on cell cytoplasm during detachment of cells studied by terahertz sensing

Blandine Lordon, Tiffany Campion, Laure Gibot, Guilhem Gallot

ABSTRACT Trypsin is a very common enzyme used in cell culture to harvest cells by cleaving the proteins responsible for cell adhesion. However, trypsin also induces undesirable effects on cells, such as altering membrane proteins and cytoskeleton, changing the composition of the cytoplasm and the cell volume, and even leading to cell death when used improperly. Using attenuated total reflection in the terahertz domain, confocal microscopy and propidium iodide test, we quantified in real time the change in cytoplasmic content induced by trypsin proteolysis on Madin-Darby canine kidney (MDCK1) epithelial cells. We have observed a cytoplasmic modification from the very first seconds of trypsinization, following the change of cell volume due to mechanical re-equilibrium of the membrane. We found that the cytoplasmic alteration is associated with a transfer of small solutes: electrolytes and metabolites. We also found a very good non-linear correlation between the side effects monitored by terahertz sensing and the cell height, regardless of the dependence of the cell height on trypsin concentration and exposure time.

SIGNIFICANCE Trypsin, commonly used in cell culture to detach cells by cleaving adhesion proteins, can adversely affect cells, impacting their membrane proteins, cytoskeleton, cytoplasmic composition, volume, and even viability. Research using attenuated total reflection in the terahertz domain alongside confocal microscopy has quantified these effects in real time. Results demonstrate that trypsin initiates cytoplasmic modifications almost immediately, which correlates with cell volume adjustments and membrane mechanical re-equilibrium. Furthermore, a significant non-linear correlation was established between these side effects and cell height, independent of trypsin concentration and exposure duration. This study highlights the complex and rapid cellular responses to trypsinization, suggesting a need for careful application to preserve cell integrity in research and therapeutic contexts.

Manuscript submitted to **Biophysical***Journal*

Article

Impact of trypsin on cell cytoplasm during detachment of cells studied by terahertz sensing

Blandine Lordon[1], Tiffany Campion[2], Laure Gibot[2], and Guilhem Gallot[1,*]

[1]LOB, Ecole polytechnique, CNRS, INSERM, Institut Polytechnique de Paris, Palaiseau, France

[2]Laboratoire Softmat, Université de Toulouse, CNRS UMR 5623, Université Toulouse III – Paul Sabatier

[*]Correspondence: Guilhem.Gallot@polytechnique.edu

INTRODUCTION

Trypsin, a pancreatic serine protease, is used daily in biology for subculturing cells during passage or for preparing cells for flow cytometry (1). Trypsin cleaves peptide bonds of proteins responsible for cell adhesion (cell-cell and cell-substrate adhesion), leaving the cells in suspension. Although highly effective for this type of process, trypsinization has numerous side effects on cells. The main reason is that trypsin undifferentiatedly hydrolyzes proteins with an arginine or lysine residue that is not followed by proline, and such termination is common to many membrane proteins. Thus, trypsin has been shown to induce many changes at the level of the cell membrane and cytoplasm. If the incubation time is too long, trypsinization may result in the loss of cell membrane proteins due to excessive enzymatic degradation, which can interfere with surface marker analysis and reduce cell viability, especially that of stem cells (2). Several groups have also shown that trypsin induces the formation of microvilli (fine, cylindrical cell extensions) on the surface of epithelial cells (3, 4); this is thought to be the cell's way of dealing with excess cell membrane as the cell becomes rounded. Detachment of the cells from the substrate also induces a change in cell morphology: the cells detach from each other and from the substrate, their volume increases and their spreading area decreases (5). Trypsin alters the cytoskeleton structure and integrity (6) that may ultimately lead to the death of the cell (5, 7). The detachment of cells from the substrate also disrupts the organization of actin filaments and cortical microtubules, leading to a change in cell stiffness and osmotic balance (8).

While trypsin is widely used in cell culture, its impact on the molecular alteration of the cytoplasm has received less attention. Molecular uptake during trypsinization was observed by Lemons *et al* in the late 1980s in fibroblasts using ^{125}I-BSA or [^{14}C]leucine (9). Papers have also documented trypsin-induced leakage of metabolites across the plasma membrane during treatment (10), possibly associated with cytoskeletal disorganization (11). Thus, trypsin may trigger transfer of molecules through the membrane by several means: ion channels and pumps, exo- and endocytosis, vesicles, resulting in a net change in the molecular composition of the cytoplasm (12–14). Understanding the dynamics of cytoplasmic modification during trypsinization is therefore interesting to minimize cell damage during the process. The techniques previously used have been

mostly destructive: mass spectroscopy (15), gas chromatography and mass spectroscopy (10), radio-labeled elements and centrifugation (9) or removal of extracellular medium (16).

Many techniques are available to investigate the dynamics of the cytoplasm content in living cells: mass spectroscopy (16), gas chromatography (10), exclusion tests (17), fluorescence and Raman spectroscopy (18, 19), protein assays (20), scanning electrochemical microscopy (21), bioluminescence (22), ICP-OES and ion chromatography (23). The terahertz domain offers many advantages, in particular allowing quantitative and non destructive investigation on living cells (19, 29, 30). Unlike the visible domain, it is directly sensitive to the content of the cytoplasm, in particular ions, metabolites and proteins. Absorption is much less important than in the infrared, and it offers better sensitivity than the hyperfrequency region (24). Recent work has demonstrated the ability to spectroscopically study complex systems such as cells and even tissues or small organs (24–29). In particular, we have shown that terahertz attenuated total reflection (THz-ATR) can follow the cytoplasmic dynamics of live monolayer epithelial MDCK1 cells in real time, without any markers, sample preparation or destruction, and with a sensitivity at least ten times better than standard fluorescence microscopy using a propidium iodide (PI) intercalating fluorescent probe (30). Terahertz measurements are very complementary to classic measurements such as the invasive ionic, ATP or LDH measurements used in this latest study. Therefore, we present here the terahertz response of cells during trypsinization. Using additional confocal microscopy experimental data, PI penetration monitoring by videomicroscopy to address plasma membrane integrity during trypsinization, and with a model of the ATR/cell sensor, we show the possibility of disentangling the geometrical cell modification linked to cell detachment and cytoplasmic contributions to the measured terahertz ATR signal. The molecular exchange across the plasma membrane was then followed in real time, and dynamic parameters were studied for various trypsin concentrations. The correlation between cytoplasmic alterations and cell detachment was investigated to answer the important question of whether it is safer to use a low concentration of trypsin for a long time, or to reduce the exposure time to a high concentration of trypsin, in order to minimize the side effects of mandatory trypsinization for cell biology experiments.

MATERIALS AND METHODS

Cell growth

Madin-Darby canine kidney (MDCK1) cells (Sigma-Aldrich, 00062106 MDCK-I) were used. MDCK1 are adherent cells with an epithelial morphology that grow as a monolayer. When the cells form a confluent monolayer, the thickness is approximately $7 \pm 2\mu$m (31). The culture medium consists of Dulbecco's modified Eagle's medium (ThermoFisher Scientific, 10566016) supplemented with 10% fetal bovine serum (DMEM, ThermoFisher Scientific, 10500064) and 1% penicillin-streptomycin (ThermoFisher Scientific, 15140122). To pass the MDCK1 cells, we expose them to a concentration of 10 μM (i.e 250 mg/L) of trypsin/EDTA (ThermoFisher Scientific, R001100) during 7 minutes. The cells were then seeded onto either glass coverslips (for confocal measurements) or silicon plates (for terahertz measurements). The cell seeding density was 31,250 per cm^2, counted with a Malassez hemocytometer. Cells were grown to confluence for 48 h and washed twice with Phosphate-Buffered saline buffer (PBS, ThermoFisher Scientific, 10010023). Before terahertz experiments, the cells are scraped from one half of the silicon plate to provide a reference signal during the terahertz measurements.

Trypsin/EDTA experiments

Trypsin/EDTA is a combination of trypsin, a protease that cleaves the peptide bonds of proteins, and ethylenediaminetetraacetate acid (EDTA), a calcium and magnesium chelator. EDTA is added to trypsin to improve its efficiency in weakening cell-cell adhesion and to increase trypsin's access to peptide bonds targeted for hydrolysis. In the different experiments, we dilute trypsin/EDTA with PBS to reach the required concentrations of 0.5 to 8 μM. As a digestive enzyme, trypsin exhibits optimal activity at 37°C (32).

Propidium iodide penetration

Plasma membrane defects were visualized using propidium iodide (Merck #P4170, Darmstadt, Germany) thanks to videomicroscopy. PI is a non-permeant fluorescent DNA intercalant, meaning penetration occurs only inside cells presenting loss of plasma membrane integrity. Briefly, 20,000 MDCK1 cells grown for 48 h in 96-well plates until reaching 95% of confluency were washed twice with PBS without Ca^{2+} and Mg^{2+} and then incubated with 100 µl of trypsin / EDTA (8 μM) containing 1 μM PI. Plates were then immediately placed within an IncuCyte S3 (Sartorius). Pictures in phase and red fluorescence were acquired every 5 min during 2 h, with quantification performed using software linked to the videomicroscope. SI.Movie1 shows cell morphological aspect and penetration of PI into cells during incubation with trypsin.

THz-ATR measurements

A vertically-polarized 3 mW, 2.5 THz continuous-wave beam (Lytid, TeraCascade 1000), collimated to 4 mm full width at half maximum is passed through the prism made of high-resistivity silicon (HR-Si, n = 3.42) in an ATR configuration (see Fig. 1). An evanescent wave extends at the interface between the top of the prism and the sample. Provided that the thickness of the cell layer matches the penetration depth of the evanescent wave, the reflected terahertz wave is correlated with the terahertz relative permittivity of the cell layer in contact with the top of the prism. The origin of the terahertz contrast was found to be related to the modification of the dielectric constant of liquid water in the presence of solutes such as ions, peptides or proteins (33). In our experiments, the thickness of the cell layer is 7 ± 2μm, which agrees well with a penetration depth of 8 μm at 2.5 THz. The THz-ATR sensor then allows real-time and continuous measurement of the change in the cell cytoplasm concentration with a time resolution of a few seconds. To achieve a high stability of the measurement, a dual frequency optical chopper splits the main beam into two halves, which are chopped simultaneously at two different frequencies (29). The upper and lower halves of the beam are modulated, relative to a master frequency set at 65 Hz, at frequencies of ×6 (390 Hz) and ×5 (325 Hz), respectively. Both halves are then subjected to ATR on the HR-Si prism, in two separate positions, where the cell sample and reference liquid are placed. After leaving the prism, both parts of the parallel beam are focused on a pyroelectric detector (Lytid, TeraPyro). The pyroelectric signal, resulting from the superposition of the two modulations, is demodulated by two independent lock-in amplifiers driven by each of the two frequencies provided by the chopper controller (SRS, SR540). One obtains the signals S_5 (×5) and S_6 (×6) for both modulations. The whole setup is placed in a sealed box with controlled humidity (below 1% relative humidity) and temperature (21±0.5°C). The ATR prism is also precisely thermalized at 37 ± 0.01°C using thermoelectric Peltier coolers and a temperature controller (Thorlabs, TED200C). To cancel out the residual fluctuations, the

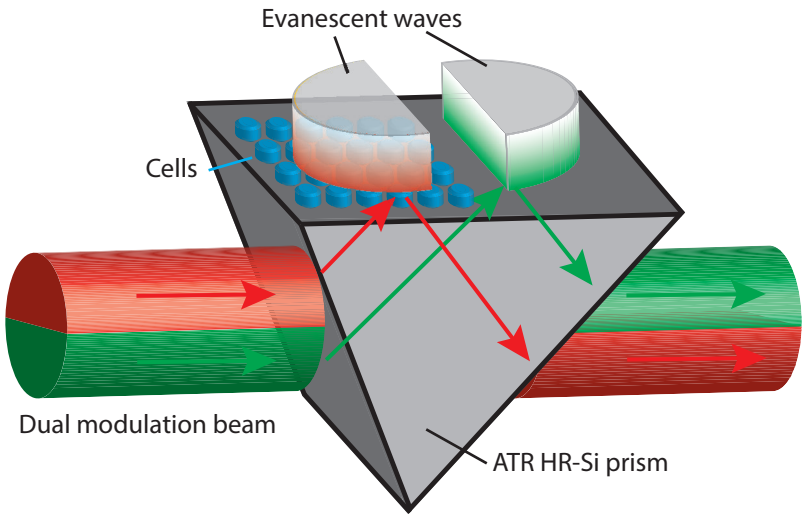

Figure 1: **THz-ATR device**. Two modulated beams arrive on the HR-Si prism in ATR configuration. Both beams induce an evanescent field above the prism (red and green gradient areas). A confluent layer of epithelial cells is placed in one of the evanescent fields. The other evanescent field is used as a reference. The reflected beam then takes into account the changes in the evanescent field induced by the sample, normalized to that of the reference.

THz signal S_{THz} used for the measurements is calculated as $S_{THz} = S_5/S_6$. The THz-ATR sensor is therefore characterized by an excellent signal-to-noise ratio and long-term stability ($< 10^{-3}$). Since the ATR prism cannot be easily removed, the MDCK1 cells were grown on a separate 3 mm thick HR-Si plate which is placed on top of the ATR prism. The area probed by the evanescent field measures around 20 mm^2. A small drop of α-pinene (Sigma-Aldrich, P45702) is used as an index matching layer to ensure the optical continuity between the prism and the cell plate.

Confocal measurements

We used a confocal microscope (Leica, TCS SP8 X) to obtain the volume of the monolayer of confluent MDCK1 cells. Cell labeling was performed with fluorescent CellTracker Orange CMTMR (ThermoFisher Scientific, C2927). It freely passes through the cell plasma membrane into the cytoplasm, where it is converted into plasma membrane impermeant molecules. It is stable and non-toxic under working conditions. The excitation peak is at 552 nm, and the emission peak is at 580 nm. The final dye concentration was 0.5 µM, diluted in a solution of PBS. For staining, the culture medium was removed, the CellTracker Orange solution was added and the cells were incubated for 35 min at 37°C with 5% CO_2 controlled atmosphere. Afterwards, the slips were then washed twice with PBS, placed on a plate holder and covered with the PBS solution. During confocal imaging, the temperature was set at 37°C. The field of view was 291,2 x 291,2 µm (0.085 mm^2) ; stacks were acquired with a height step of 0.5 µm, over a range of 20 µm. First, we acquire a reference volume of the cell layer. Then, trypsin/EDTA is added at the required concentration and we record a XYZ volume of the cell layer every minute for 15 minutes.

RESULTS AND DISCUSSION

We studied the phenomenon of trypsin proteolysis using the terahertz sensor with the aim of quantifying trypsin-induced cytoplasmic content dynamics. We hypothesized that the terahertz signal depends on two different contributions: a contribution resulting from induced morphological changes because of progressive cell detachment, and a contribution resulting from cytoplasmic modification because of hypothetical plasma membrane defects caused by enzymatic (over)activity (duration of incubation, concentration...). For measurements with the THz-ATR sensor, a silicon plate with confluent MDCK1 cells was placed on the HR-Si prism and covered with 1 mL PBS. The terahertz signal R_{THz} was recorded for 15 min to check the stability and to let the temperature of the medium stabilize at 37°C and for normalization purpose ($t < 0$, blue zone Fig. 2A). At $t = 0$, a concentrated solution of trypsin/EDTA in PBS was added to reach the required trypsin concentration. The solution was pumped in and out several times to homogenize the solution around the cells. We then recorded the THz-ATR signal for an additional 30 min (green zone Fig. 2A). Finally, the cells were scraped off the silicon plate to provide a reference for normalization (yellow zone Fig. 2A). We chose trypsin concentrations between 0.5 and 8 μM, corresponding to the lower range of concentrations classically used in cell culture. However, the dynamics directly obtained by the THz-ATR sensor potentially takes into account both the cytoplasm and the morphological contributions, since the terahertz sensing by the evanescent wave is localized close to the ATR prism surface.

Therefore, to determine the morphological contribution induced by trypsin proteolysis, we used confocal microscopy on confluent MDCK1 cells. Cells were grown and stained with CellTracker Orange. They were then placed on a plate holder and covered with 1 mL PBS and exposed to a controlled atmosphere at 37°C. A reference volume was acquired with the confocal microscope using a 0.5 μm z-step. A concentrated solution of trypsin/EDTA in PBS was then added to the medium surrounding the cells to achieve the required trypsin concentration from 1 to 8 μM. Fig. 2B1 shows the reference stack cross-section and Fig. 2B2 the trypsinized cells for a concentration of 5 μM for 15 min. The intensity distribution of the fluorophore along the z-direction is then calculated by summation. A double Gaussian fit is applied to the intensity distribution. The first Gaussian is narrow and located close to the microscope slide, corresponding to residual dye molecules at the slide interface. This peak is found to be stationary along the trypsinization. In contrast, the second peak is much larger and is related to the cells that detach from the slide. It gives the averaged cell height $H(t)$ along z. This height is calculated at each time interval (Δt = 1 min) during 15 min (see figure 2C). It corresponds to the morphological contribution of trypsin proteolysis on the MDCK1 cells. The smallest change corresponds to a trypsin concentration of 1 µM. Starting from 2 µM, the cell height increases rapidly during the first minutes after trypsin addition and then reaches a plateau after about 10 min. Exponential growth functions fit the data well, as shown by the solid lines in Fig. 2C. These changes in cell morphology, i.e round shaping and detachment, was also seen by videomicroscopy (SI.Movie1).

To analyze the terahertz data, and to disentangle the geometrical and cytoplasmic contributions, we model the experimental setup (see Fig. 3) as a multilayer system : the HR-Si prism, the cell monolayer, and the extracellular medium considered as infinite above the cells. Each layer is characterized by its optical relative permittivity at 2.5 THz. The reflection coefficient R from the ATR prism is calculated for p-polarization, corresponding to the laser polarization, from the Fresnel reflection coefficient of a multilayer optical system (34). The reflection coefficient R from the ATR prism is calculated for p-polarization, corresponding to the laser polarization, from the Fresnel reflection coefficient of a multilayer optical system (34). It depends on

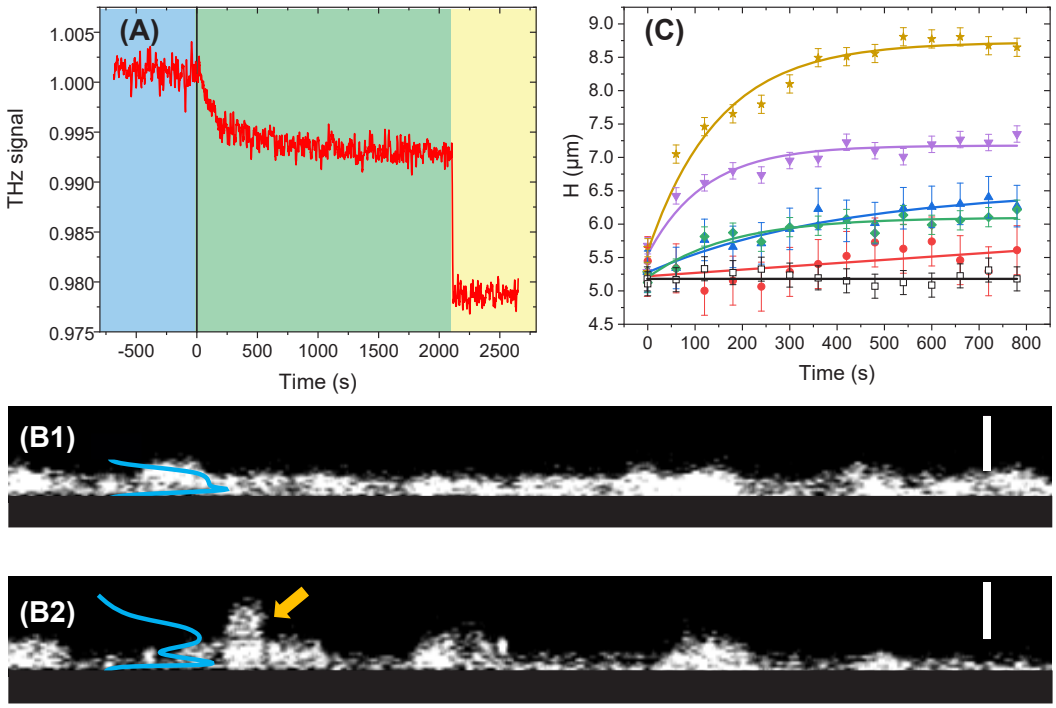

Figure 2: **Experimental data**. **(A)** THz-ATR acquisition during trypsinization of MDCK1 cells with a trypsin/EDTA concentration of 5 µM. The signal is divided into 3 zones. The left blue zone is a stabilization phase in PBS ; the middle green zone is the dynamic of the signal during trypsin proteolysis, trypsin/EDTA being added at $t = 0$; the right yellow zone is the signal after scraping the cells off the silicon plate. **(B)** Confocal microscopy on MDCK1 cells, transverse view. (B1) Layer of confluent MDCK1 cells stained with CellTracker Orange. (B2) Layer of the same cells but trypsinized for 15 min with a concentration of 5 µM. The blue curve shows the dye intensity distribution. The yellow arrow indicates a cell that detached from the substrate. The scale bar is 20 μm. **(C)** Evolution of the thickness of the MDCK1 cell layer as a function of time during trypsinization for different concentrations evaluated by confocal microscopy. The dots are the measured width of the intensity distribution of the CellTracker Orange dye staining the cytosol. The solid lines correspond to an exponential growth fit. Black curve is the control; red = 1 µM; blue = 2 µM; green = 3.5 µM; purple = 5 µM; orange = 8 µM.

the permittivity and on the thickness and confluency of the cell layer, and is then potentially modified by the trypsin/EDTA proteolysis. Previous studies showed that the permittivity of the solutes in the terahertz range mainly depends on their molar mass M, so that the cytoplasm permittivity is the averaged of the permittivity of each solute, weighted by its terahertz response (33, 35).

The parameters of the model are introduced in Table 1. We define the cytoplasm and medium complex permittivities by ϵ_c and ϵ_m, respectively. The difference $\Delta\epsilon = \epsilon_c - \epsilon_m$ is obtained by

$$\Delta\epsilon(t) = \frac{1}{V_c(t)} \int D(t, M)\, \alpha(M)\, \mathrm{d}M = \frac{\alpha_T(t)}{V_c(t)}, \tag{1}$$

where V_c is the probed volume of cytoplasm, α is the solute polarizability, D is the molar distribution of the solutes in the cytoplasm, and α_T is the total polarizability. Then, we define the fraction of cytoplasm content variation f from the physiological

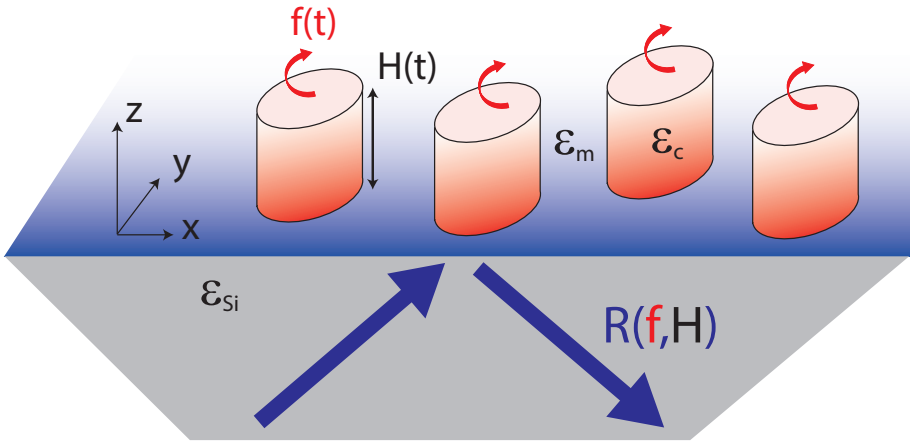

Figure 3: **Multilayer model** to compute the reflection coefficient as a function of the height of the cell layer $H(t)$ and the fraction of cytoplasm content variation $f(t)$. The blue arrows show the incident and reflected terahertz beams. The red arrows show the change of cytoplasmic content. The blue gradient represents the evanescent field.

Table 1: List of parameters.

Parameter	**Symbol**
Cell height	H
Cytoplasm, medium and total probed surfaces	S_c, S_m, S_T
Probed volume of cytoplasm	$V_c = H \cdot S_c$
Cytoplasm, medium, silicon and effective permittivity	$\epsilon_c, \epsilon_m, \epsilon_{\text{Si}}, \epsilon_{\text{eff}}$
Fraction of cytoplasm content variation	f

conditions at time $t = 0$ by $\alpha_T(t) = f(t)\,\alpha_T(0)$.

We now introduce ϵ_{eff} the complex permittivity of the area probed by the evanescent wave. Before the addition of trypsin/EDTA at time $t = 0$, ϵ_{eff} is a function of the total surface probed S_T and the complex permittivity of the medium and of the cytoplasm, respectively ϵ_m and ϵ_c. Using the Gladstone-Dale equation (36), the effective permittivity $\epsilon_{\text{eff}} = \frac{1}{S_T}\left[\epsilon_c S_c + \epsilon_m S_m\right]$, where S_c and S_m are the respective probed surfaces of cytoplasm and medium, satisfying the relationship $S_m + S_c = S_T$. Thus $\epsilon_{\text{eff}} = \frac{1}{S_T}\left[\epsilon_c S_c + \epsilon_m (S_T - S_c)\right]$.

Using equation 1 and the relationship $V_c = H \cdot S_c$ where H is the cell layer height, one obtains

$$\begin{aligned}\epsilon_{\text{eff}} &= \frac{1}{S_T}\left[S_c(\epsilon_m + f(t)\frac{\alpha_T(0)}{V_c(t)}) + \epsilon_m(S_T - S_c)\right] \\ &= \epsilon_m[1 + \delta(t)] \quad \text{with} \quad \delta(t) = f(t)\frac{\alpha_T(0)}{\epsilon_m H(t) S_T}.\end{aligned} \tag{2}$$

This result may seem surprising since ϵ_{eff} does not depend explicitly on cell volume, but only on two parameters: the change in cytoplasm $f(t)$ and the height of the cell layer $H(t)$. This is due to the particularity of the terahertz device, which is based on the evanescent field along the direction of the z-axis at the surface of the prism, which breaks the symmetry of the volume (see Fig. 3). This means that the terahertz signal remains constant when the cells are spread out, as long as the solute molecules

remain at the same distance from the prism surface, i.e. along the (xy) plane.

Going back to the model and using the Fresnel equation for a multilayer system (34), we compute the reflection coefficient from the ATR prism R_{THz} as the product between R_0 and a function of H, ϵ_{Si}, ϵ_{eff} and ϵ_m. The proportionality coefficient R_0 takes into account the unknown constant transmission coefficient of the whole system apart from the ATR prism.

The permittivity of silicon is known $\epsilon_{Si} = 11.7$ (37), the one of the medium is very close to the one of water and also well known (38). The normalization procedure is in two steps. First, R_0 is obtained from empty cell data, where $f = 0$ (see zone 3, yellow, in Fig. 2A). Second, R_{THz} is compared to the experimental data without trypsin/EDTA (zone 1, blue, in Fig. 2A at $t < 0$) where $f = 1$. We compute δ_0 in ϵ_{eff} so that $R(\delta_0) = R_{\text{THz}}(t < 0)$, and then the effective permittivity writes

$$\epsilon_{\text{eff}} = \epsilon_m \left[1 + \delta_0 \, f(t) \frac{H_0}{H(t)} \right], \tag{3}$$

where H_0 is the cell height at rest without trypsin/EDTA. Therefore, the only remaining unknown parameters are $f(t)$ and $H(t)$. Finally, we can discuss the influence of the molar mass of the molecules involved in the terahertz signal, taken into account the variation of the solute polarizability α in the effective permittivity (Eq.1) and subsequently in R_{THz}. As described in more details in the Supplementary Information (Fig.SI1), small solutes such as the one found in PBS have a negative contribution to the measured terahertz signal. On the contrary, it is positive for bigger molecules such as proteins.

We now introduce $R_p(x, H)$, the theoretical reflected signal calculated using the model described in the Materials and Methods section; its inputs are the height of the MDCK1 layer H, and the fraction of cytoplasm content f (see Fig. 3). Knowing $H(t)$ from the confocal measurements, we can calculate $f(t)$ such that $R_{THz} = R(f, H)$ for each trypsin concentration. Raw terahertz measurements were used for R_{THz}, while exponential fits were used for $H(t)$ to minimize fluctuations. The evolution of $f(t)$ is shown in figure 4A. We observe a decay of f on the first 200 s followed by a plateau. The contribution of the geometrical contribution to the total terahertz signal is about 25% for total cell detachment. The dynamics are typical exponential behavior. A mono exponential decay fit $f_0 + A\, e^{-t/T}$ was performed to obtain the amplitude of the decay A and the characteristic decay time T. Figure 4B shows the evolution of A and of the decay rate $\gamma = 1/T$ versus trypsin concentration. We observe an important increase of both A and γ with trypsin concentration. The modification of cytoplasm is weak for the lower concentration at 0.5 μM corresponding to about 10% of the variation in cytoplasm content. It reaches 30% for a trypsin concentration of 8 μM. The magnitude of the changes in the characteristic decay time is even larger, by a factor 10. It ranges from 33±5 s at 8 μM to 320±50 s at 1 μM concentrations.

Since f is only due to a change in the number of molecules in the cytoplasm, molecular transfer may occur in and out of the cells. We monitored the penetration of propidium iodide (PI) by confocal videomicroscopy (see Fig. 5), which showed negligible PI entry, at least 100 times lower than the control with saponin, the reference for creating pores in the plasma membrane (39). This test excludes the permeabilization of molecules bigger than PI (690 Da). However, Dettmer *et al* (10) observed significant metabolite leakage in the SW480 adenocarcinoma cell line, after trypsin/EDTA treatment using GC-MS. All these metabolites have a mass of between 90 and 340 Da. They also observed the release of the amino acids alamine and ornithine with a characteristic time of about 10 min, which is consistent with that observed for f (Fig. 4B). Furthermore, the change in cell volume observed during trypsinization is associated with cell membrane expansion and the flattening of microvilli (finger-like projections with actin cores) or membrane folds, and with a change in membrane stiffness and actin microfilament structure (40). This unfolding is also balanced by endo- and exocytosis (41, 42). Venkova et al. (43) demonstrated

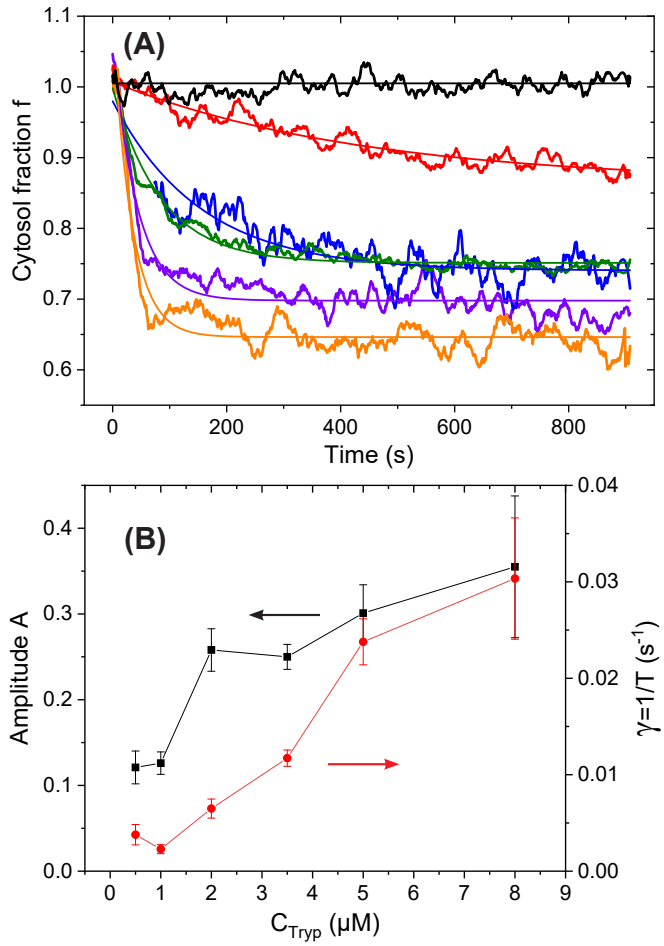

Figure 4: **Dynamics of cell cytoplasm content**. **(A)** Fraction of cytoplasm content $f(t)$ for different concentrations of trypsin/EDTA. Black curve is the control (3); red = 1 µM (6); green = 3.5 µM (3); purple = 5 µM (5); orange = 8 µM (3). () is the number of samples. **(B)** Parameters of the exponential decay fit of $f(t)$ for the different trypsin/EDTA concentrations $f_0 + A\ e^{-t/T}$. The black square curve represents the amplitude A of the decay; the red curve is the decay rate $\gamma = 1/T$.

the existence of a mechano-osmotic coupling that defines a membrane tension homeostasis operating in cells, causing volume fluctuations associated with rapid changes in cell shape, with potential consequences for cell physiology. Volume variations of up to 20% have been observed, implying a homeostatic response of the cell and therefore a transfer of electrolytes across the cell membrane. These observations can explain the observed decrease in the terahertz signal. Firstly, the entry into the cytoplasm of ions from the PBS solution surrounding the cells leads to a decrease in the signal since the contribution of these small inorganic ions is negative, as previously discussed (see also the Supplementary Information, Figs.SI1 and SI2). Secondly, the exit of amino acids and small peptides from the cytoplasm also leads to a decrease in signal since their contribution to the signal is positive. The molar mass of such molecules, as determined by Dettmer *et al* (10), is less than 240 Da, and is therefore consistent with the PI exclusion tests (Fig. 5).

We then further investigate the following question: is it safer to use a high concentration of trypsin for a short time, or to increase the exposure time to a low concentration of trypsin, in order to minimize the cytoplasmic side effects of trypsinization?

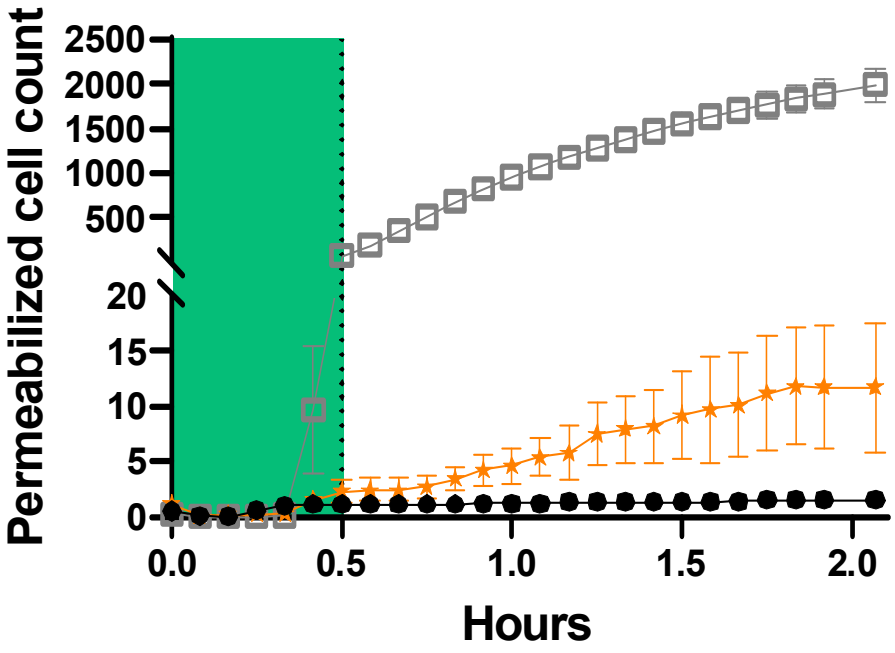

Figure 5: **Monitoring the penetration of propidium iodide** by videomicroscopy after incubation of MDCK1 cells with 8 µM trypsin (orange star, ⋆). The green zone represents the dynamics of the signal during the first 30 min of exposure to trypsin proteolysis, as monitored by terahertz radiation in Figure 2. Saponin detergent (grey square, □) is used as a positive control for membrane permeabilization. The negative control (no trypsin) are black dots, •. For each $n = 5$.

In other words, what is the intrinsic role of trypsin concentration on cytoplasmic alteration side effects? We proceed as follows. At each investigated trypsin/EDTA concentration and from the recorded dynamics of $x(t)$ and $H(t)$, we can calculate for a given time delay t_1 the corresponding values of cell height variation $\Delta H = H(t_1) - H_0$ and the cytoplasm content variation $\Delta x = 1 - x(t_1)$. The results are shown in Fig. 6 for 5 time delays from 80 to 300 s and for 6 concentrations from 0.5 to 8 μM, and show a remarkable non linear correlation between Δx and ΔH ($R^2 \approx 0.98$) with the fitting equation $\Delta f = 0.332(1 - e^{-\Delta H/0.655})$. The points define a regular curve independent of the concentration. This means that when a given cell detachment is obtained during trypsinization, the cytoplasm modification is always the same regardless of the trypsin/EDTA concentration used, at least in the concentration range used in this study. Therefore, the same cytoplasmic side effect is expected, whether a low concentration of trypsin is used for a long time or a high concentration is used for a short time. It is interesting to note that, in the range of trypsin concentrations studied here, the impact on the cell depends essentially on the total number of trypsin molecules encountered by the cell, independently of the temporal arrival of these molecules. This implies that the effect of trypsin/EDTA seems to be very tolerant in the sense that a reasonably large range of trypsin concentration can be used to achieve the same results on the cells. This is in agreement with the cell culture procedures.

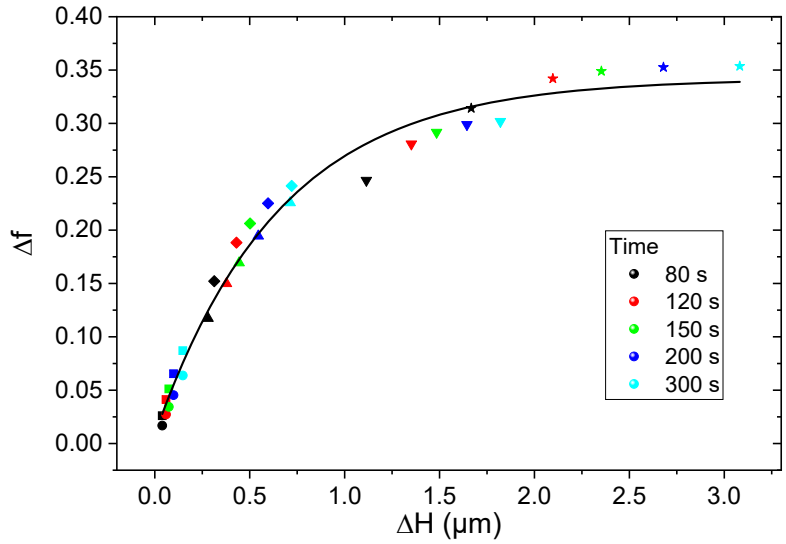

Figure 6: **Correlation between the fraction of cytoplasm and the cell height**. Cytoplasm content variation Δf versus cell height variation ΔH for 5 identical time delays from 80 to 300 s and for 6 trypsin/EDTA concentrations. The dot colors refer to the time delays as indicated in the legend. The dot shapes refer to concentrations at 0.5 (circle •), 1 (square ▪), 2 (up triangle ▲), 3.5 (diamond ◆), 5 (down triangle ▼) and 8 μM (star, ★). The solid line is an exponential growth function fit $\Delta f = 0.332(1 - e^{-\Delta H/0.655})$.

CONCLUSION

In this article, the modification of the cytoplasmic content as a side effect of cell detachment during trypsinization was studied in real time by THz, confocal microscopy and videomicroscopy measurements. Using the geometric data obtained from confocal microscopy and a model of the cell/sensor interaction, THz-ATR sensing proved to be a very interesting technique to obtain real-time quantitative data on cytoplasmic dynamics due to the action of trypsin/EDTA on the membrane proteins. A significant modification of the cytoplasmic content was observed during the first minutes after the addition of trypsin/EDTA, whose amplitude and dynamic rate increase sharply with the trypsin concentration. This modification can be explained both by the entry of inorganic ions from the extracellular PBS solution, and by the leakage of amino acids and small peptides from the cytoplasm. Interestingly, we found a very good non-linear correlation between the cytoplasm alteration and the cell height, regardless of the dependence of the cell height on trypsin concentration and exposure time. This may explain why the cell culture procedures found in the literature are tolerant to the concentrations to be used.

FUNDING

This research was funded by the French Agence Nationale de la recherche (ANR-11-EQPX-0029 and ANR-21-CE42-0018).

AUTHOR CONTRIBUTIONS

B. Lordon carried out the terahertz experiments. T. Campion performed the videomicroscopy measurements. B. Lordon and G. Gallot carried out the modeling and calculations. B. Lordon, L. Gibot and G. Gallot wrote the article. G. Gallot designed the research.

DECLARATION OF INTEREST

The authors declare no competing interests.

REFERENCES

1. Campbell, N., 2016. Biology. Pearson, 11th edition.

2. Fischer, B., A. Meier, A. Dehne, A. Salhotra, T. A. Tran, S. Neumann, K. Schmidt, I. Meiser, J. C. Neubauer, H. Zimmermann, and L. Gentile, 2018. A Complete Workflow for the Differentiation and the Dissociation of hiPSC-derived Cardiospheres. *Stem Cell Research* 32:65–72.

3. Harrison, C., and T. Allen, 1979. Cell Surface Morphology After Trypsinisation Depends on Initial Cell Shape. *Differentiation* 15:61–66.

4. Furcht, L., and G. Wendelschafer-Crabb, 1978. Trypsin-Induced Coordinate Alterations in Cell Shape, Cytoskeleton, and Intrinsic Membrane Structure of Contact-Inhibited Cells. *Experimental Cell Research* 114:1–14.

5. Yan, J., C. Xie, J. Zhu, Z. Song, Z. Wang, and L. Li, 2021. Effect of Trypsin Concentration on Living SMCC-7721 Cells Studied by Atomic Force Microscopy. *Journal of Microscopy* 284:203–213.

6. Raizada, M. K., G. Tan, and R. E. Fellows, 1981. Trypsin-induced alterations of insulin binding, microfilament organization and cell shape in fibroblastic cultures from non-diabetic and diabetic mice. *Experimental Cell Research* 133:261–271.

7. Nowak-Terpilowska, A., P. Sledzinski, and J. Zeyland, 2021. Impact of Cell Harvesting Methods on Detection of Cell Surface Proteins and Apoptotic Markers. *Brazilian Journal of Medical and Biological Research* 54:e10197.

8. Nehls, S., H. Nöding, S. Karsch, F. Ries, and A. Janshoff, 2019. Stiffness of MDCK II Cells Depends on Confluency and Cell Size. *Biophysical Journal* 116:2204–2211.

9. Lemons, R., S. Forster, and J. Thoene, 1988. Protein Microinjection by Protease Permeabilization of Fibroblasts. *Analytical Biochemistry* 172:219–227.

10. Dettmer, K., N. Nürnberger, H. Kaspar, M. A. Gruber, M. F. Almstetter, and P. J. Oefner, 2011. Metabolite Extraction from Adherently Growing Mammalian Cells for Metabolomics Studies: Optimization of Harvesting and Extraction Protocols. *Analytical and Bioanalytical Chemistry* 399:1127–1139.

11. Liu, X., S. Oh, and M. W. Kirschner, 2022. The Uniformity and Stability of Cellular Mass Density in Mammalian Cell Culture. *Frontiers in Cell and Developmental Biology* 10:1017499.

12. Cadart, C., L. Venkova, P. Recho, M. C. Lagomarsino, and M. Piel, 2019. The Physics of Cell-Size Regulation across Timescales. *Nature Physics* 15:993–1004.

13. Hapala, I., 1997. Breaking the Barrier: Methods for Reversible Permeabilization of Cellular Membranes. *Critical reviews in biotechnology* 17:105–122.

14. Stewart, M. P., A. Sharei, X. Y. Ding, G. Sahay, R. Langer, and K. F. Jensen, 2016. In Vitro and Ex Vivo Strategies for Intracellular Delivery. *Nature* 538:183–192.

15. Ziemanski, JF., JZ. Chen, and KK. Nichols, 2020. Evaluation of Cell Harvesting Techniques to Optimize Lipidomic Analysis from Human Meibomian Gland Epithelial Cells in Culture. *International journal of molecular sciences* 21.

16. Vogel, K. G., 1978. Effects of Hyaluronidase, Trypsin, and EDTA on Surface Composition and Topography during Detachment of Cells in Culture. *Experimental Cell Research* 113:345–357.

17. Stoddart, J. M., 2011. Mammalian Cell Viability: Methods and Protocols. Humana Press.

18. Rols, M. P., and J. Teissie, 1990. Electropermeabilization of Mammalian Cells. Quantitative Analysis of the Phenomenon. *Biophys J* 58:1089–1098.

19. Azan, A., M. Grognot, T. García-Sánchez, L. Descamps, V. Untereiner, O. Piot, G. Gallot, and L. M. Mir, 2020. Monitoring the Molecular Composition of Live Cells Exposed to Electric Pulses via Label-Free Optical Methods. *Scientific Reports* 10:10471.

20. Walker, J. M., 2009. The Protein Protocols Handbook. Springer Protocols Handbooks. Humana Press.

21. Koley, D., and A. J. Bard, 2010. Triton X-100 Concentration Effects on Membrane Permeability of a Single HeLa Cell by Scanning Electrochemical Microscopy (SECM). *Proceedings of the National Academy of Sciences* 107:16783–16787.

22. Champiat, D., A. Roux, O. Lhomme, and G. Nosenzo, 1994. Biochemiluminescence and Biomedical Applications. *Cell Biology and Toxicology* 10:345–351.

23. Wouters, B., C. Bruggink, G. Desmet, Y. Agroskin, C. A. Pohl, and S. Eeltink, 2012. Capillary Ion Chromatography at High Pressure and Temperature. *Analytical Chemistry* 84:7212–7217.

24. Masson, J. B., M. P. Sauviat, J. L. Martin, and G. Gallot, 2006. Ionic Contrast Terahertz near Field Imaging of Axonal Water Fluxes. *Proc Natl Acad Sci USA* 103:4808–4812.

25. Shiraga, K., Y. Ogawa, T. Suzuki, N. Kondo, A. Irisawa, and M. Imamura, 2014. Characterization of Dielectric Responses of Human Cancer Cells in the Terahertz Region. *Journal of Infrared Millimeter and Terahertz Waves* 35:493–502.

26. Yu, C., S. Fan, Y. Sun, and E. Pickwell-MacPherson, 2012. The Potential of Terahertz Imaging for Cancer Diagnosis: A Review of Investigations to Date. *Quant Imaging Med Surg* 2:33–45.

27. Woodward, R. M., B. E. Cole, V. P. Wallace, R. J. Pye, D. D. Arnone, E. H. Linfield, and M. Pepper, 2002. Terahertz Pulsed Imaging in Reflection Geometry of Human Skin Cancer and Tissue. *Phys. in Med. and Biol.* 47:3853–3863.

28. Masson, J.-B., M.-P. Sauviat, and G. Gallot, 2006. Ionic Contrast Terahertz Time Resolved Imaging of Frog Auricular Heart Muscle Electrical Activity. *Appl. Phys. Lett.* 89:153904.

29. Grognot, M., and G. Gallot, 2015. Quantitative Measurement of Permeabilization of Living Cells by Terahertz Attenuated Total Reflection. *Appl. Phys. Lett.* 107:103702.

30. Zheng, X., B. Lordon, A.-F. Mingotaud, P. Vicendo, R. Brival, I. Fourquaux, L. Gibot, and G. Gallot, 2023. Terahertz Spectroscopy Sheds Light on Real-Time Exchange Kinetics Occurring through Plasma Membrane during Photodynamic Therapy Treatment. *Advanced Science* 2300589.

31. Cho, M., and D. Thompson, 1987. The Madin Darby Canine Kidny (MDCK) epithelial cell monolayer as a model cellular - transport barrier. *Journal of Pharmaceutical Sciences* 76:S49.

32. Sipos, T., and J. Merkel, 1970. Effect of calcium ions on the activity, heat stability, and structure of trypsin. *Biochemistry* 9:2766–2775.

33. Grognot, M., and G. Gallot, 2017. Relative Contributions of Core Protein and Solvation Shell in the Terahertz Dielectric Properties of Protein Solutions. *J. Phys. Chem. B* 121:9508–9512.

34. Born, M., and E. Wolf, 1980. Chapter II - Electromagnetic Potentials and Polarization. *Principles of Optics (Sixth Edition)* 71–108.

35. Zheng, X., T. Gevart, and G. Gallot, 2021. High Precision Dual-Modulation Differential Terahertz ATR Sensor for Liquid Measurements. *Opt Lett* 46:4045–4048.

36. Reis, J. C. R., I. M. S. Lampreia, Â. F. S. Santos, M. L. C. J. Moita, and G. Douhéret, 2010. Refractive Index of Liquid Mixtures: Theory and Experiment. *ChemPhysChem* 11:3722–3733.

37. Dai, J., J. Zhang, W. Zhang, and D. Grischkowsky, 2004. Terahertz Time-Domain Spectroscopy Characterization of the Far-Infrared Absorption and Index of Refraction of High-Resistivity, Float-Zone Silicon. *J. Opt. Soc. Am. B* 21:1379–1386.

38. Ronne, C., P.-O. Astrand, and S. R. Keiding, 1999. THz Spectroscopy of Liquid H2O and D2O. *Phys. Rev. Lett.* 82:2888–2891.

39. Francis, G., Z. Kerem, H. P. S. Makkar, and K. Becker, 2002. The Biological Action of Saponins in Animal Systems : A Review. *British Journal of Nutrition* 88:587.

40. Figard, L., and A. M. Sokac, 2014. A Membrane Reservoir at the Cell Surface: Unfolding the Plasma Membrane to Fuel Cell Shape Change. *BioArchitecture* 4:39–46.

41. Groulx, N., F. Boudreault, S. N. Orlov, and R. Grygorczyk, 2006. Membrane Reserves and Hypotonic Cell Swelling. *Journal of Membrane Biology* 214:43–56.

42. Masters, T. A., B. Pontes, V. Viasnoff, Y. Li, and N. C. Gauthier, 2013. Plasma Membrane Tension Orchestrates Membrane Trafficking, Cytoskeletal Remodeling, and Biochemical Signaling during Phagocytosis. *Proceedings of the National Academy of Sciences* 110:11875–11880.

43. Venkova, L., A. S. Vishen, S. Lembo, N. Srivastava, B. Duchamp, A. Ruppel, A. Williart, S. Vassilopoulos, A. Deslys, J. M. Garcia Arcos, A. Diz-Muñoz, M. Balland, J.-F. Joanny, D. Cuvelier, P. Sens, and M. Piel, 2022. A Mechano-Osmotic Feedback Couples Cell Volume to the Rate of Cell Deformation. *eLife* 11:e72381.